Vibration Characteristics of Pretwisted Aerofoil Cross-Section Blade Packets Under Rotating Conditions

M. Sabuncu*
Dokuz Eylül University, Bornova-Izmir, Turkey
and
J. Thomas†
University of Surrey, Guildford-Surrey, England, United Kingdom

Turbine blades are usually pretwisted and have asymmetric cross sections. Furthermore, turbine blades are formed into packets by joining them at critical locations with shrouds or lacing. Such a procedure alters the vibration characteristics of the blade. In this paper, the free vibration characteristics of rotating, shrouded, pretwisted aerofoil cross-section blade packets are investigated using a finite element model. One end of the pretwisted blade is assumed to be fixed at the periphery of a disk rotating about its center, whereas the other end of the blade is connected by a curved shroud. Expressions for kinetic and strain energies of a pretwisted blade packet subjected to centrifugal force are derived. Shear deformation and rotary inertia effects are neglected in the analysis. The effects of pretwist, stagger angle, rotational speed, shroud length, shroud thickness, shroud width, and the distance of shear center from the centroid on the vibration characteristics of blade packets are investigated. Comparisons made between theoretical and experimental results show very good agreement.

Nomenclature

A = area of blade cross section
A_s = area of shroud cross section (curved beam)
b = axial thickness of the curved beam
C = torsional stiffness
C_c = torsional constant
C_f = center of flexure
cg = center of blade cross section
d_X, d_Y = coordinates of center of flexure with respect to principal axis
d_x, d_y = coordinates of center of flexure with respect to fixed axis system
E = modulus of elasticity
E_s = modulus of elasticity of shroud materials (curved beam material)
G_s = shear modulus of shroud material
g = gravitational acceleration
I_{cf} = polar moment of inertia per unit length about center of flexure
I_{cg} = polar moment of inertia per unit length about centroid
I_{XX} = second moment of area of cross section about XX
I_{xx} = second moment of area of cross section about x_1x_1
I_{xxs} = second moment of area of shroud cross section about XX
I_{xy} = product moment of area of cross section about x_1x_1 and y_1y_1
I_{YY} = second moment of area of cross section about YY
I_{yy} = second moment of area of cross section about y_1y_1
I_{yys} = second moment of area of shroud cross section about YY
i = rotation of the tangent of curved beam, $(\partial w/\partial y) - V/R$
$i, i+1$ = node numbers of a typical beam element
J = slope of u deflection of a curved beam, $-\mathrm{d}u/\mathrm{d}y$
J_{xxs} = St. Venant torsion constant of shroud
(K_s) = stiffness matrix of stationary beam element
k = counter
L = blade length, Lagrangian function
L_r = shroud length to blade length ratio, (L_{sh}/L)
L_{sh} = total length of curved beam
l = length of beam element
l_{sh} = curved beam element length
M = mass matrix of beam, number of elements along the curved beam
(m_i) = mass matrix of beam element
N = number of elements
p = frequency
q = element coordinate vector
q_i = generalized displacements for an in-plane element
q_o = generalized displacements for an out-of-plane element
R = distance between centroid and center of flexure
(R_i) = stiffness matrix of beam element due to rotation
r = disk radius
S = stiffness matrix of beam
(S_i) = stiffness matrix of beam element
T = kinetic energy
t = time, radial thickness of a curved beam
u = displacements of center of flexure in x direction
u_f = strain energy due to centrifugal effects
u_1 = displacements of centroid in x_1 direction
V = strain energy
V_s = strain energy of stationary beam
v = displacement of center of flexure in y direction

Received Sept. 22, 1989; revision received Nov. 29, 1990; accepted for publication Nov. 29, 1990.

*Associate Professor in Vibrations, Department of Mechanical Engineering.
†Lecturer in Vibrations, Department of Mechanical Engineering.

v_1 = displacement of centroid in y_1 direction
w = weight of blade per unit length, displacement of center of flexure in z direction
w_s = weight of shroud resting on each blade
XX,YY = principal axes through centroid of blade cross section
xx,yy = coordinates axes through center of flexure of blade cross section
x_1x_1,y_1y_1 = coordinates axes through centroid of blade cross section
Z = coordinate distance measured along undeflected blade from root
ZZ = longitudinal axis
α = angle between coordinates axes (x_1x_1,y_1y_1) and principal axes (XX,YY), angle of pretwist
β = subtended angle of each curved beam element
β_* = pretwist angle along the beam element
γ = position angle (due to the pretwist)
γ_* = flexural rigidity ratio of shroud to blade, (E_sI_s/EI)
Δ_* = weight ratio of shroud to blade, $(\rho_sA_s/\rho A)$
$\delta\delta$ = coordinate axis through centroid of blade cross section parallel to plane of disk
θ = torsional displacement
θ = nodal coupled coordinate vector between X and θ
λ = frequency parameter of the beam AL^4p^2/EI
$\xi\xi$ = coordinate axis through centroid of blade cross section perpendicular to plane of disk
ρ_s = density of shroud
ϕ = angle between axes $\xi\xi,\delta\delta$ and axes x_1x_1,y_1y_1, stagger angle of blade
ϕ_i = pretwist angles of each beam element at their starting points
ω = angular velocity of rotation of disk
$\{\ \}$ = denotes column matrix
$(\ )^T$ = denotes transpose of a matrix
$(\ )^{-1}$ = denotes inverse of matrix

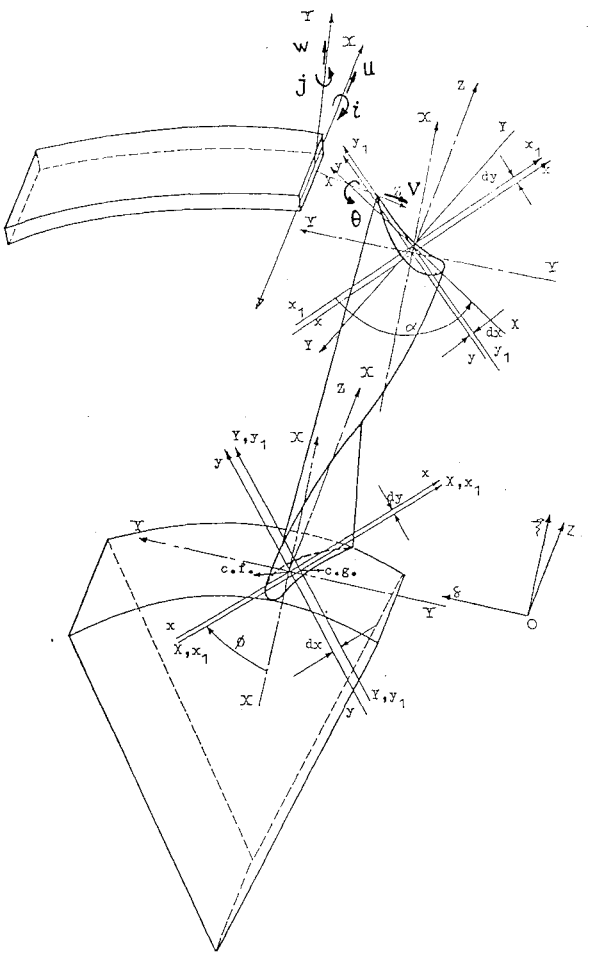

Fig. 1 Local and global coordinates of a section of a pretwisted blade packet.

Introduction

STODOLA,[1] in 1927, and Sezawa,[2] in 1933, studied the vibration of blade packets, but due to the algebraic complexity of the equations, exact solutions were not sought. Later, Prohl[3] used the step-by-step Holzer's method to obtain the frequencies of a packet. In his analysis, the blades were considered fixed at the root and a packet was idealized by stations of lumped masses, forces, and moments. Although the shear center and centroid of the blade cross sections were assumed coincident, the axial and torsional vibrations were coupled through the shroud. Vibrations in the plane of the disk remained uncoupled.

Thomas and Belek[4] studied the free vibration characteristics of straight shrouded blade packets using the finite element method. Thomas and Sabuncu[5] studied the dynamic analysis of rotating asymmetric cross-section blade packets using the finite element method. One end of the blade was assumed to be fixed at the periphery of a disk rotating about its center, whereas the other end of the blade was connected to a curved shroud. The effect of various parameters such as the shroud dimensions, stagger angle, rotational speed, disk radius, and distance of shear center from the centroid on the vibration characteristics of blade packets were systematically presented.

Thomas and Sabuncu[6] developed a finite element model for the dynamic analysis of an asymmetric cross-section blade. The blade was assumed to be fixed at the periphery of a disk rotating at constant angular velocity. The effects of rotational speeds and stagger and pretwist angles on the vibration characteristics were investigated.

Ewin's work[8] consisted of a study of a very simplified mass-spring model made as a preliminary investigation of the general vibration characteristics of a packeted assembly. Ewins and Imregun[9] investigated the vibrational behavior of turbine blades when grouped into packets. Two methods of analysis based on substructuring via receptance coupling were developed and used with success to predict the natural frequencies of a 30-bladed disk with various packeting arrangements. A series of experiments were conducted on a special test piece to confirm these predictions.

Table 1 Details of pretwisted two-bladed packet used in the experiment where blades have aerofoil cross section (N_B = 2; N = 6; M = 5; disk radius r_2 = 8 in.)

Blades	
Blade cross section	A = 0.00914 in.^{2}
Blade length	L = 6 in.
Stagger angle	ϕ = 0 deg
Pretwist angle	α = 45 deg
Young's modulus	E = 31.0 × 10^6 lb/in.^{2}
Blade density	ρ = 0.283 lb/in.^{3}
Second moment of inertia	I_{XX} = 0.000084 in.^{4} I_{YY} = 0.00671 in.^{4}
Shear center distance from centroid	d_X = 0.0076 in. d_Y = 0.047 in.
Torsional rigidity	C = 3240 lbf in.
Increment of torsional rigidity	C_c = 392 lbf.
Shroud	
Shroud thickness	t = 1/16 in.
Shroud width	b = 1/2 in.
Young's modulus	E_s = 31.0 × 10^6 lb/in.^{2}
Shroud length	L_{sh} = 4.39823 in.
Shroud density	ρ_s = 0.283 lb/in.^{3}

In the past, investigations have been directed toward analyzing the vibration characteristics of rectangular cross-section blade packets. In Ref. 5, the more complex configuration of an asymmetric aerofoil cross-section blade packet has been investigated. The effect of rotation has also been considered. Turbine blades encountered in practice have a pretwisted asymmetrical aerofoil cross section. Because of the complex configuration of the blade cross section, the problem becomes more difficult to analyze, as coupling between bending-bending-torsional vibrations takes place and also because of the shroud interaction. When a curved beam is used as a shroud, out-of-plane bending and torsional displacements are coupled. Hence, none of the modes of the assembly are independent.

In order to verify the approach, a finite element model is applied to various problems. Theoretical results obtained by the finite element method are compared with experimental results since there are no results available in the existing literature. The effect of rotational speed on the vibration characteristics is also considered.

Energy Expression of a Pretwisted Blade Packet

The strain energies of a blade vibrating under nonrotating and rotating conditions are derived for blades joined together by a shroud. This packet is rigidly fixed at the periphery of a disk rotating at constant angular velocity. As mentioned in Ref. 5, there is an increase in strain energy due to the rotation in a single blade. This strain energy increase is also increased by the centrifugal force of the rotating shroud mass.

Strain Energy of a Shrouded-Blade Element in a Centrifugal Field

The strain energy equation of a rotating, shrouded, pretwisted blade element can be written in dimensional form for the kth element as

$$
\begin{aligned}
V = {} & \int_0^l \left[\frac{EI_{yy}}{2}\left(\frac{\partial^2 U}{\partial x^2}\right)^2 + EI_{xy}\left(\frac{\partial^2 V}{\partial z^2}\right)\left(\frac{\partial^2 U}{\partial Z^2}\right) + \frac{EI_{xx}}{2}\left(\frac{\partial^2 V}{\partial Z^2}\right)^2 \right. \\
& \left. + \frac{C}{2}\left(\frac{\partial \theta}{\partial Z}\right)^2 + \frac{EA}{2}\left(\frac{\partial W}{\partial Z}\right)^2 \right] dz \\
& + \frac{\omega^2 A\rho}{2}\int_0^l [r_2 + (k-1)l + C_{sh1} + Z]\left[\int_0^l \left(\frac{\partial U_1}{\partial Z_1}\right)^2 dZ_1 \right. \\
& \left. + \int_0^l \left(\frac{\partial U_2}{\partial Z_2}\right)^2 dZ_2 + \cdots + \int_0^l \left(\frac{\partial U_k}{\partial Z_k}\right)^2 dZ_k \right] dZ_k \\
& + \frac{\omega^2 A\rho}{2}\int_0^l [r_2 + (k-1)l + C_{sh1} + Z] \int_0^l \left[\left(\frac{\partial V_1}{\partial Z_1}\right)^2 dZ_1 \right. \\
& \left. + \int_0^l \left(\frac{\partial V_2}{\partial Z_2}\right)^2 dZ_2 + \cdots + \int_0^l \left(\frac{\partial V_k}{\partial Z_k}\right)^2 dZ_k \right] dZ_k \\
& - \frac{\omega^2 A\rho}{2}\int_0^l (U_1^2 \sin^2\phi \\
& - 2U_1 V_1 \sin\phi\cos\phi + V_1^2 \cos^2\phi)\, dZ \\
& + C_{sh2}\int_0^l (U_1 U_{\max}^T \sin^2\phi - U_{\max} V_1^T \sin\phi\cos\phi \\
& - V_{\max} U_1^T \sin\phi\cos\phi + V_1 V_{\max}^T \cos^2\phi)\, dz \qquad (1)
\end{aligned}
$$

where

$$C_{sh1} = \frac{\omega_s R}{w} \qquad C_{sh2} = \frac{\omega_s}{2w}$$

Table 2 Comparison of experimental and theoretical values of pretwisted two-aerofoil cross-section bladed packet[a]

Mode number	Frequency, Hz		
	Theoretical	Experimental	% error
1	88.5	92.0	−3.8
2	389.9	380.0	2.6
3	395.3	405.0	−2.3
4	643.0	656.0	−2.0
5	912.4	868.0	5.0
6	975.8	—	—
7	1396.5	1305.0	6.9
8	1506.1	1483.0	1.5
9	1780.6	—	—
10	1894.3	—	—
11	2114.7	1993.0	6.1
12	2529.6	2505.0	0.9
13	2851.3	2775.0	2.7
14	3049.4	3140.0	−2.8
15	3707.0	3879.0	−4.4

[a]Details of the blade packet are given in Table 1.

The pretwist along the blade length can be written in dimensional form as

$$\gamma = (k-1)\frac{\alpha}{L}l + \frac{\alpha}{L}Z \qquad (2)$$

where k is the order number of the element.

By using the relationship between I_{xx}, I_{yy} and I_{XX}, I_{YY} given in Ref. 6,

$$I_{xx} = (S - H\cos 2\gamma)\, I_{XX} \qquad (3)$$

$$I_{yy} = (S + H\cos 2\gamma)\, I_{XX} \qquad (4)$$

$$I_{xy} = H\sin 2\gamma I_{XX} \qquad (5)$$

where

$$S = \frac{1}{2}\left(\frac{I_{YY}}{I_{XX}} + 1\right)$$

$$H = \frac{1}{2}\left(\frac{I_{YY}}{I_{XX}} - 1\right)$$

Also, d_x, d_y are given in Ref. 6 as

$$d_x = d_X \cos(\beta_* Z + \phi_i) - d_Y \sin(\beta_* Z + \phi_i) \qquad (6)$$

$$d_y = d_X \sin(\beta_* Z + \phi_i) - d_Y \cos(\beta_* Z + \phi_i) \qquad (7)$$

The displacement functions assumed are third-order polynomials for U, V and linear for θ, W. That is,

$$U = V = \sum_{r=0}^{3} a_r Z^r \qquad (8a)$$

$$\theta = w = \sum_{r=0}^{r=1} C_r Z^r \qquad (8b)$$

Substituting from Eqs. (2–8) into the strain energy V, the strain yields a discretized strain energy of a blade in the form:

$$V = \frac{\frac{1}{2}EI_{XX}}{L^3}\{q\}^T[S_i]\{q\} \qquad (9)$$

where

$$\{q\} = [u_1 u_1' u_2 u_2' v_1 v_1' v_2 v_2' \theta_1 \theta_2 w_1 w_2]^T \qquad (10)$$

$$[S_i] = [C^*]^{-T}[k_r][C^*]^{-1}$$

$$[C^*]^{-1} = \begin{bmatrix} [C] & 0 & 0 & 0 \\ 0 & [C] & 0 & 0 \\ 0 & 0 & [\tilde{k}] & 0 \\ 0 & 0 & 0 & [\tilde{k}] \end{bmatrix}$$

$$[C] = \begin{bmatrix} 1 & 0 & 0 & 0 \\ 0 & 1 & 0 & 0 \\ -\frac{3}{l^2} & -\frac{2}{l} & \frac{3}{l^2} & -\frac{1}{l} \\ \frac{2}{l^3} & \frac{1}{l^2} & -\frac{2}{l^3} & \frac{1}{l^2} \end{bmatrix}$$

$$[\tilde{k}] = \begin{bmatrix} 1 & 0 \\ -\frac{1}{l} & \frac{1}{l} \end{bmatrix}$$

$k_r(1,1) = SS\,A1$, $k_r(1,2) = SS\,A2$, $k_r(1,3) = SS\,A3$

$k_r(1,4) = SS\,A4$, $k_r(1,5) = CS\,A1$, $k_r(1,6) = CS\,A2$

$k_r(1,7) = CS\,A3$, $k_r(1,8) = CS\,A4$

$k_r(1,9) = TS\,R15 + RS\,I15$, $k_r(1,10) = TS\,R16 + RS\,I16$

$k_r(2,2) = SS\,A3 + A1\psi + A23$

$k_r(2,3) = SS\,A4 + 2\psi A2 + A34$

$k_r(2,4) = SS\,A5 + 3\psi A3 + A45$, $k_r(2,5) = CS\,A2$

$k_r(2,6) = CS\,A3$, $k_r(2,7) = CS\,A4$, $k_r(2,8) = CS\,A5$

$k_r(2,9) = TS\,R25 + RS\,I25 + H(\Lambda G25 + FI25 + FS25)GC$

$k_r(2,10) = TS\,R26 + RS\,I26 + H(\Lambda G26 + \Gamma FI26 + \Gamma FS26)GC$

$k_r(3,3) = SS\,A5 + 4\psi A3 + 4/3\,A45 + AA$

$k_r(3,4) = SS\,A6 + 6\psi A4 + 1.5\,A56 + BB$, $k_r(3,5) = CS\,A3$

$k_r(3,6) = CS\,A4$, $k_r(3,7) = CS\,A5 + FF$

$k_r(3,8) = CS\,A6 + GG$

$k_r(3,9) = TS\,R35 + RS\,I35 + H(\Lambda G35 + \Gamma FI35 + FS35)GC$

$k_r(3,10) = TS\,R36 + RS\,I36 + H(\Lambda G36 + \Gamma FI36 + FS36)GC$

$k_r(4,4) = SS\,A7 + 9\psi A5 + 1.8\,A67 + DD$

$k_r(4,5) = CS\,A4$, $k_r(4,6) = CS\,A5$

$k_r(4,7) = CS\,A6 + GG$, $k_r(4,8) = CS\,A7 + HH$

$k_r(4,9) = TS\,R45 + RS\,I45 + H(\Lambda G45 + \Gamma FI45 + FS45)GC$

$k_r(4,10) = TS\,R46 + RS\,I46 + H(\Lambda G46 + \Gamma FI46 + FS46)GC$

$k_r(5,5) = CC\,A1$, $k_r(5,6) = CC\,A2$, $k_r(5,7) = CC\,A3$

$k_r(5,8) = CC\,A4$, $k_r(5,9) = TC\,I15 + RS\,R15$

$k_r(5,10) = TC\,I16 + RS\,R16$

$k_r(6,6) = CC\,A3 + \psi A1 + A23$

$k_r(6,7) = CC\,A4 + 2\psi A2 + A34$

$k_r(6,8) = CC\,A5 + 3\psi A3 + A45$

$k_r(6,9) = TC\,I25 + RS + R25 + H(\Lambda Z25 + \Gamma TI25 + TS25)GC$

$k_r(6,10) = TC\,I26 + RS\,R36 + H(\Lambda Z26 + \Gamma TI26 + TS26)GC$

$k_r(7,7) = CC\,A5 + 4\psi A3 + 4/3\,A45 + PP$

$k_r(7,8) = CC\,A6 + 6\psi A4 + 1.5\,A56 + QQ$

$k_r(7,9) = TC\,I35 + RS\,R35 + H(\Lambda Z35 + \Gamma TI35 + TS35)GC$

$k_r(7,10) = TC\,I36 + RS\,R36 + H(\Lambda Z36 + \Gamma TI36 + TS36)GC$

$k_r(8,8) = CG\,A7 + 9\psi A5 + 1.8\,A67 + RR$

$k_r(8,9) = TC\,I45 + RS\,R45 + H(\Lambda Z45 + \Gamma TI45 + TS45)GC$

$k_r(8,10) = TC\,I46 + RS\,R46 + H(\Lambda Z46 + \Gamma TI46 + TS46)GC$

$k_r(9,9) = TC\,I55 + TS\,R55 + 2\,RS\,Y55 + H[(Z55 + G55) + TI55 + FI55) + TS55 + FS55]GC$

$k_r(9,10) = TC\,I56 + TS\,R56 + 2\,RS\,Y56 + H[\Lambda(Z56 + G56) + (TI56 + FI56) + TS56 + FS56]GC$

$k_r(10,10) = TC\,I66 + TS\,R66 + 2RS\,Y66 + H[\Lambda(Z66 + G66) + (TI66 + FI66) + TS66 + FS66]GC + CT\,A1$

$k_r(12,12) = CL\,A1$

where

$RT + I_{XX}/I_{YY}$, $CT = (C + C_c\beta_*^2)/(EI_{XX})$, $CL = A/I_{XX}$

$\Lambda = \Lambda + [r_2 A1 + 2\,A2(k-1)]/L^3 + A2/L^3 + L_3(tbR^2 - \beta_*\pi)/(180\,A\rho A1)\rho_s$

$\Gamma = [r_2 A1 + (k-1)2\,A2]/L^3 + L^3(tbR^2\beta_*\rho_s\pi)/(180\,A\rho)$

$\psi = \Lambda H$, $H = (\rho A\omega^3)/(EgI_{XX})$, $GC = L^3$, $TC = CC\,L^3$

$TS = SS\,L^3$, $RS = CS\,L^3$, $CC = -H\,0.5(1 - \cos 2\phi)$

$SS = -H\,0.5(1 + \cos 2\phi)$, $CS = H\,0.5\sin 2\phi$, $A1 = lL^3$

$$A2 = L^3l^2/2, \quad A3 + L^3l^3/3, \quad A4 = L^3l^4/4, \quad A5 = L^3l^5/5$$

$$A6 = L^3l^6/6, \quad A7 = L^3l^7/7, \quad A23 = H(\Gamma A2 + A3)$$

$$A34 = H(\Gamma A3 + A4), \quad A45 = H(\Gamma A4 + A5)$$

$$A56 = H(\Gamma A5 + A6), \quad A67 = H(\Gamma A6 + A7)$$

Kinetic Energy of a Blade Element

The kinetic energy expression of a pretwisted blade element under combined bending-torsional vibrations is given in dimensional form in Ref. 6. Using Eqs. (6) and (7) to obtain the variation of the distance of the flexure center from the centroid along the length of the blade due to pretwist, and also for the representation of the displacement Eq. (8), substituting into the kinetic energy equation and replacing the coefficients, the kinetic energy of a blade element becomes

$$T = \frac{\rho A L p^2}{2} \{q\}^T [m_i] \{q\} \tag{11}$$

where

$$[m_i] = [C^*]^{-T} [m] [C^*]^{-1} \tag{12}$$

The matrix $[C^*]^{-1}$ is given in Eq. (10). The matrix form and elements of $[m]$ are given as

$$[m] = \begin{bmatrix} K1 & K2 & K3 & K4 & & & V1 & V2 & & \\ & K3 & K4 & K5 & & & V2 & V3 & & \\ & & K5 & K6 & 0 & & V3 & V4 & 0 & \\ & & & K7 & & & V4 & V5 & & \\ & & & & K1 & K2 & K3 & K4 & U1 & U2 \\ & \text{symmetric} & & & K3 & K4 & K5 & U2 & U3 & 0 \\ & & & & & K5 & K6 & U3 & U4 & \\ & & & & & & K7 & U4 & U5 & \\ & & & & & & 0 & 0 & 0 & 0 \\ & & & & & & & C_\theta & 0 & 0 \\ & & & & & & & & 0 & 0 \\ & & & & & & & & & K1 \end{bmatrix} \tag{13}$$

Table 3 Details of pretwisted two-bladed packet used in the experiment, where blades have aerofoil cross section (N_B = 2; N = 6; M = 5; disk radius r_2 = 9.927 in.)

Blades	
Blade cross section	A = 0.0914 in.^{2}
Blade length	L = 6 in.
Stagger angle	ϕ = 30 deg
Pretwist angle	α = 30 deg
Young's modulus	E = 31.0 10^6 lb/in.^{2}
Blade density	ρ = 0.270 lb/in.^{3}
	I_{XX} = 0.000084 in.^{4}
Second moment of inertia	I_{YY} = 0.00671 in.^{4}
	d_X = 0.0076 in.
Shear center distance from centroid	d_Y = 0.047 in.
Torsional rigidity	C = 3240 lbf in.
Increment of torsional rigidity	C_c = 392 lbf
Shroud	
Shroud thickness	t = 0.0625 in.
Shroud width	b = 0.25 in.
Young's modulus	E_s = 31.10^6 lb/in.^{2}
Shroud length	L_{sh} = 4.16967 in.
Shroud density	ρ_s = 0.270 in.^{3}

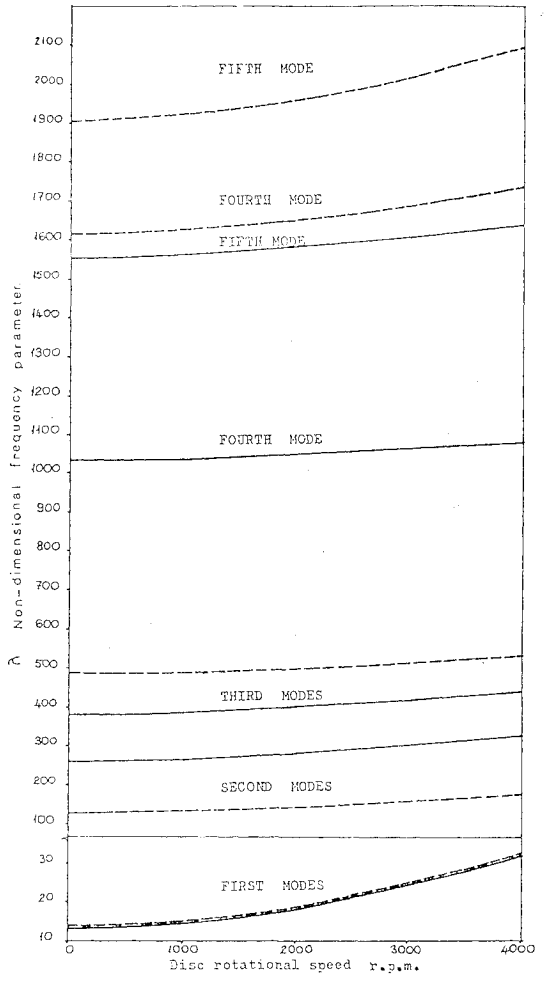

Fig. 2 Effect of disk rotational speed on the nondimensional frequency parameters of various pretwisted blade packets: L_r = 0.2; t = 1/32 in.; b = 1 in.; — α = 45 deg; --- α = 90 deg.

where

$$K1 = l/L, \quad K2 = l^2/2L, \quad K3 = l^3/3L$$

$$K4 = l^4/4L, \quad K5 = l^5/5L, \quad C_\theta = \frac{I_{cf}}{LA}$$

$$S = \sin\theta_i, \quad C = \cos\theta_i, \quad A9 = S\,CO1 + C\,SI1$$

$$B9 = C\,CO1 - SI1, \quad C9 = S\,CO2 + C\,SI2$$

$$D9 = C\,CO2 - S\,SI2, \quad E9 = S\,CO3 + C\,SI3$$

$$F9 = C\,CO3 - S\,SI3, \quad G9 = S\,CO4 + C\,SI4$$

$$H9 = C\,CO4 - S\,SI4, \quad I9 = S\,CO5 + C\,SI5$$

$$J9 = C\,CO5 - S\,SI5, \quad V1 = d_XA9 + d_YB9$$

$$V2 = d_XC9 + d_YD9, \quad V3 = d_XE9 + d_YF9$$

$$V4 = d_XG9 + d_YH9, \quad V5 = d_XI9 + d_YJ9$$

$$U1 = d_XB9 - d_YA9, \quad U2 = d_XD9 - d_YC9$$

$$U3 = d_XF9 - d_YE9, \quad U4 = d_XH9 - d_XG9$$

$$U5 = d_XJ9 - d_YI9$$

Curved Beam Element

In the analysis, the shroud is represented by curved beam elements. The shroud is assumed to have a rectangular cross

section; hence, in-plane and out-of-plane vibrations are dealt with separately and combined to form the shroud element. Derivation of the expression for the increase of strain energy due to centrifugal force in the plane of the disk is given in Ref. 5.

In-Plane Vibration

Deflection functions used in the analysis are given in Ref. 5 as

$$W = a_1 \cos\phi_0 + a_2 \sin\phi_0 + a_4 - a_6\phi_0 = W_* a \quad (14a)$$

$$V = a_1 \sin\phi_0 + a_2 \cos\phi_0 + a_3 + a_5\phi_0 + \tfrac{1}{2}a_6\phi_0^2 = V_* a \quad (14b)$$

where

$$\phi_0 = y/R$$

Strain Energy

The strain energy of a curved beam, in a centrifugal field, acting as a shroud attached at the tips of the rotating blades, is given in Ref. 5 as

$$V = \frac{1}{2}\left\{\int_0^l \begin{bmatrix} V_*'' - W'/R \\ V_*/R + W_* \end{bmatrix}^T \begin{bmatrix} E_s I_{xx_s} & 0 \\ 0 & E_s A_s \end{bmatrix} \times \begin{bmatrix} V_*'' - W_*'/R \\ V_*/R + W_*' \end{bmatrix}\right\} dy - \tfrac{1}{2}\rho_s\omega^2 \int_0^{l_{sh}} \int_{A_s} \left\{\left[-ZW + \frac{R+Z}{R}V\right]^2 + 2W^2\right\} dA\, dy \quad (15)$$

Using the deflection functions given in Eqs. (14) and substituting in Eq. (15) yields

$$V = \tfrac{1}{2}\{q_1\}^T [C_1]^{-T} [k_1^*] [C]^{-1} \{q_1\} \quad (16)$$

where

$$\{q_1\}^T = [v_i w_i i_i v_{i+1} w_{i+1} i_{i+1}], \qquad i = \frac{w}{y} - \frac{v}{R} \quad (17)$$

$$[C_1]^{-1} = \begin{bmatrix} -B_4 & B_1 & -R\,B_4 & -B_5 & -B_1 & -R\,B_5 \\ -B_3 & B_2 & -R\,B_3 & -B_1 & -B_2 & -R\,B_1 \\ B_1 & -B_2 & R\,B_3 & B_1 & B_2 & R\,B_1 \\ B_4 & -B_3 & R\,B_4 & B_5 & B_1 & R\,B_5 \\ B_6 & -B_7 & R\,B_8 & B_6 & B_7 & R\,B_9 \\ -B_1 & B_2 & -R\,B_1 & -B_1 & -B_2 & -R\,B_1 \end{bmatrix} \quad (18)$$

$$D = 2\cos\beta - 2 + \beta\sin\beta, \qquad B_1 = (\cos\beta - 1)/D$$

$$B_2 = \sin\beta/D, \qquad B_3 = (1 - \beta\sin\beta - \cos\beta)/D$$

$$B_4 = (\sin\beta - \beta\cos\beta)/D, \qquad B_5 = (\beta - \sin\beta)/D$$

$$B_6 = B_1\beta/2, \qquad B_7 = B_2\beta/2, \qquad B_8 = B_6 + 1/\beta$$

$$B_9 = B_6 - 1/\beta$$

$$[k_1^*] = [k_1] + [k_{sf}] \quad (19)$$

where

$$[k_l] = \frac{E_s I_{xx_s}}{R^3} \begin{bmatrix} 0 & 0 & 0 & 0 & 0 & 0 \\ & 0 & 0 & 0 & 0 & 0 \\ & & 0 & 0 & 0 & 0 \\ \text{symmetric} & & & Q\beta & Q\beta & 0 \\ & & & & \beta(1+Q) & \beta^2/2 \\ & & & & & \beta^3/3 \end{bmatrix}$$

$$Q = 12\,R^2/t^2$$

and

$$[k_{sf}] = X_1[W_r] + \frac{X_2}{2}[V_r W_r] + X_3[V_r]$$

$$X_1 = -\rho_s\omega^2\left(\frac{bt^3}{12} + 2\,bt\right)$$

$$X_2 = -\omega^2\rho_s\frac{bt^3}{24R}$$

$$X_3 = -\omega^2\rho_s\left(bt + \frac{bt^3}{12R^2}\right)$$

$$[W_r] = \begin{bmatrix} C2S & CS & 0 & C & 0 & -CI \\ & C2S & 0 & S & 0 & -S1 \\ & & 0 & 0 & 0 & 0 \\ \text{symmetric} & & & \beta & 0 & -\beta^2/2 \\ & & & & 0 & 0 \\ & & & & & \beta^3/3 \end{bmatrix}$$

$$[V_r W_r] = \begin{bmatrix} -2CS & C2S & C & -S & CI & \left(\frac{C2}{2} + SI\right) \\ & 2CS & S & C & SI & \left(\frac{S2}{2} - CI\right) \\ & & 0 & \beta & 0 & -\beta^2/2 \\ \text{symmetric} & & & 0 & \beta^2/2 & \beta^3/6 \\ & & & & 0 & -\beta^3/3 \\ & & & & & -\beta^4/4 \end{bmatrix}$$

$$[V_r] = \begin{bmatrix} S2S & -CS & -S & 0 & -SI & -\frac{S2}{2} \\ & C2 & C & 0 & CI & \frac{C2}{2} \\ & & \beta & 0 & \beta^2/2 & \beta^3/6 \\ \text{symmetric} & & & 0 & 0 & 0 \\ & & & & \beta^3/3 & \beta^4/8 \\ & & & & & \beta^5/20 \end{bmatrix}$$

$$C2S = 0.5(\beta + 0.5\sin 2\beta), \qquad CS = 0.25(\cos 2\beta - 1)$$

$$C = \sin\beta, \qquad CI = \cos\beta - 1 + \beta\sin\beta$$

$$C2 = 2\beta\cos\beta + (\beta^2 - 2)\sin\beta$$

$$S2S = 0.5(\beta - 0.5\sin 2\beta), \qquad S = -(\cos\beta - 1)$$

$$SI = \sin\beta - \beta\cos\beta$$

$$S2 = 2\beta\sin\beta + 2(\cos\beta + 1) - \beta^2\cos\beta$$

Kinetic Energy

The kinetic energy expression of a curved beam under combined bending-bending displacements is given in Ref. 5 as follows:

$$T = \tfrac{1}{2}\{\dot{q}_I\}^T\{C_I\}^{-T}\rho_s A_s \int_0^{l_{sh}} \left\{ \begin{bmatrix} V_* \\ W_* \end{bmatrix}^T \begin{bmatrix} V_* \\ W_* \end{bmatrix} \right\} dy[C_I]^{-1}\{\dot{q}_I\} \tag{20}$$

Equation (20) can be written as follows:

$$T = \{\dot{q}_I\}^T[C_I]^{-T}[m_I][C_I]^{-1}\{\dot{q}_I\} \tag{21}$$

where the transformation matrix $[C_I]^{-1}$ and $\{q_I\}^T$ have been given in Eqs. (18) and (17), respectively. The mass matrix $[m_I]$ is

$$[m_I] = \rho_s A_s R \times \begin{bmatrix} \beta & 0 & \cos\beta - 1 & \sin\beta & \beta\cos\beta - \sin\beta & C_o \\ & \beta & \sin\beta & 1 - \cos\beta & \cos\beta + \sin\beta - 1 & C_1 \\ & & \beta & 0 & \beta^2/2 & \beta^3/6 \\ & \text{symmetric} & & \beta & 0 & -\beta^2/2 \\ & & & & \beta^3/3 & \beta^4/8 \\ & & & & & \beta^5/20 + \beta^3/3 \end{bmatrix} \tag{22}$$

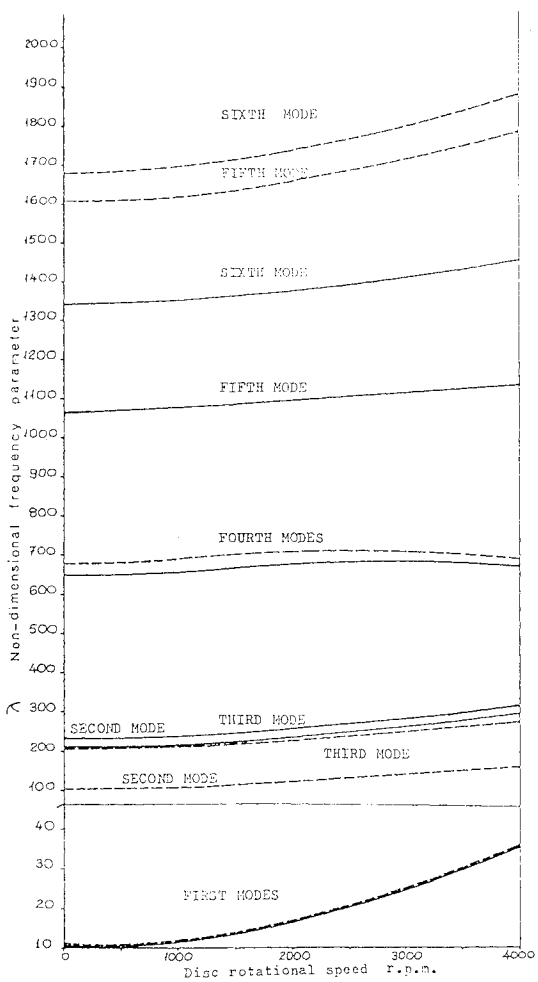

Fig. 3 Effect of disk rotational speed on the nondimensional frequency parameters of various pretwisted blade packets: L_r = 0.5; t = 1/32 in.; b = 1 in.; — α = 45 deg; --- α = 90 deg.

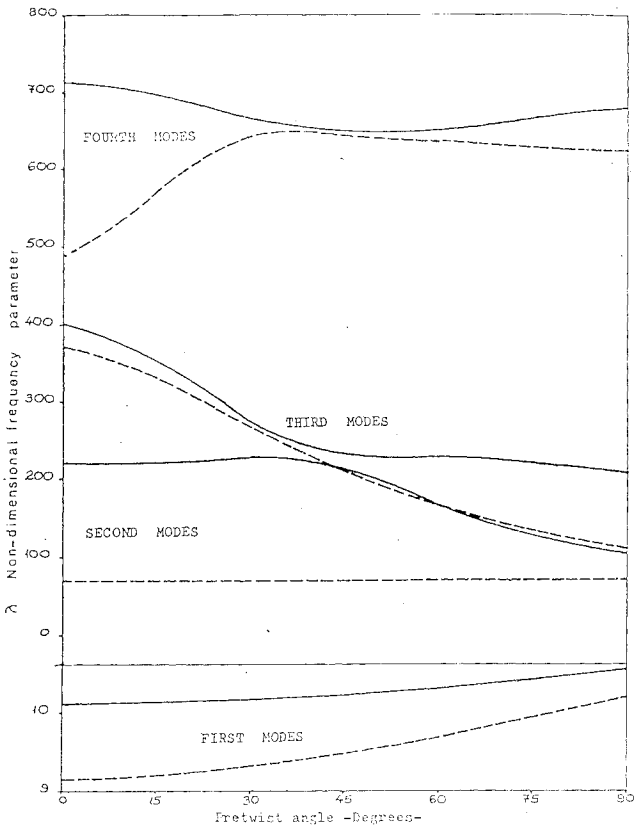

Fig. 4 Pretwist angle effect on the nondimensional frequency parameters of various staggered, pretwisted blade packets: L_r = 0.5; --- ϕ = 90 deg; — ϕ = 0 deg.

where

$$C_o = (\beta^2 - 4)\cos\beta/2 - 2\beta\sin\beta + 2$$

$$C_1 = (\beta^2 - 4)\sin\beta/2 + 2\beta\cos\beta$$

Out-of-Plane Vibration

Deflection functions used in the analysis are given in Ref. 5 as

$$U = a_1 R\cos\phi + a_2 R\sin\phi + a_3 R - a_4 R\phi - a_6 R\phi = U_* a$$

$$\theta = a_1\cos\phi + a_2\sin\phi - a_5 - a_6\phi = \theta_* a$$

where

$$\phi = y/R$$

Strain Energy

The strain energy of a curved beam undergoing coupled bending and torsional vibration, neglecting the shear deformation, is given in Ref. 5 as

$$V = \frac{1}{2}\{q_o\}^T[C_o]^{-T}\left\{\int_0^{l_{sh}} \begin{bmatrix} \theta_*/R + U_* \\ \theta_*^1 - U_*^1/R \end{bmatrix}^T \begin{bmatrix} E_s I_{yy_s} & 0 \\ 0 & G_s J_{xx_s} \end{bmatrix} \begin{bmatrix} \theta_*/R + U_*'' \\ \theta_*^1 - U^1/R \end{bmatrix} dy \right\}[C_o]^{-1}\{q_o\} \tag{23}$$

Equation (23) can be rewritten as

$$V = \{q_o\}^T[C_o]^{-T}[k_o][C_o^{-1}]\{q_o\} \tag{24}$$

where

$$\{q_o\}^T = [\theta_i U_i J_i \theta_{i+1} U_{i+1} J_{i+1}], \qquad J = -\frac{\partial u}{\partial y} \tag{25}$$

The stiffness matrix $[k_0]$ is given by

$$[k_o] = \frac{E_s I_{yys}}{R}\begin{bmatrix} 0 & 0 & 0 & 0 & 0 & 0 \\ & 0 & 0 & 0 & 0 & 0 \\ & & 0 & 0 & 0 & 0 \\ & \text{symmetric} & & C_2\theta & 0 & 0 \\ & & & & \beta & \beta^2/2 \\ & & & & & \beta^3/3 \end{bmatrix} \tag{26}$$

where

$$C_2 = \frac{G_s J_{yys}}{E_s I_{yys}}$$

and the transformation matrix $[C_o]^{-1}$ is given by

$$[C_o]^{-1} = \begin{bmatrix} 0 & -\beta/R & B_2 & 0 & B_1/R & B_3 \\ 0 & -B_5/R & -B_4 & 0 & B_5/R & -B_1 \\ 0 & B_4/R & -B_2 & 0 & -B_1/R & -B_3 \\ -1/\beta & 1/R\beta & 0 & 1/\beta & -1/R\beta & 0 \\ -1 & -B_1/R & B_2 & 0 & B_1/R & B_3 \\ 1/\beta & 2B_1/R\beta & -B_1 & -1/\beta & -2B_1/R\beta & -B_1 \end{bmatrix} \tag{27}$$

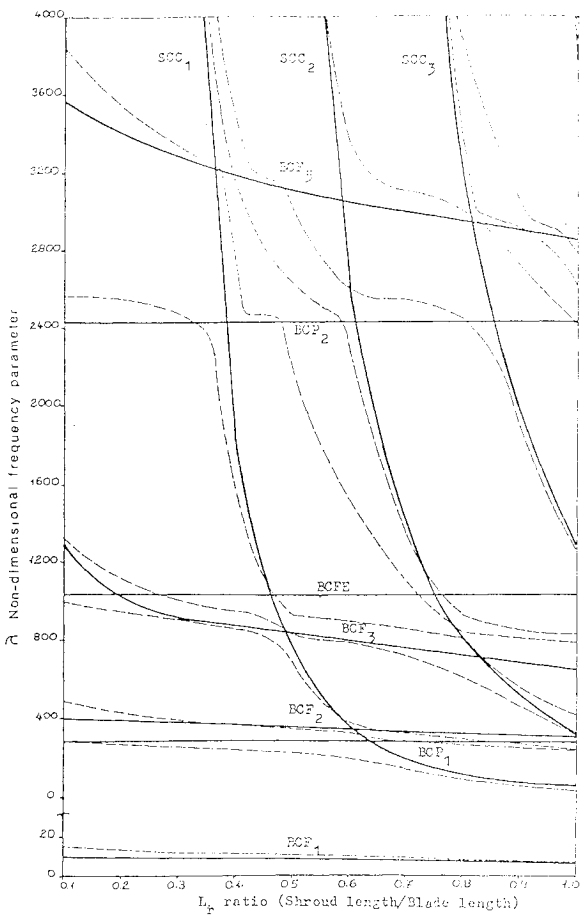

Fig. 5 In-plane and out-of-plane inference diagram of a pretwisted packet: t = 1/32 in.; b = 1.0 in.; α = 15 deg.

where

$$B_1 = (\cos\beta - 1)/D, \qquad B_2 = (\beta\cos\beta - \sin\beta)/D$$

$$B_3 = (\sin\beta - \beta)/D, \qquad B_4 = (1 - \cos\beta - \beta\sin\beta)/D$$

$$B_5 = \sin\beta/D, \qquad D = 2 - 2\cos\beta - \beta\sin\beta$$

Kinetic Energy

The kinetic energy of a curved beam undergoing combined bending and torsional displacement neglecting the rotary inertia effect is given in Ref. 5 as

$$T = \frac{1}{2}\{q_o\}^T[C_o]^{-T}\left\{\int_0^{l_s/b}\begin{bmatrix}\dot{U}_* \\ \dot{\theta}_* R\end{bmatrix}^T \times \begin{bmatrix}\rho_s A_s & 0 \\ 0 & Ip/A_s R^2\end{bmatrix}\begin{bmatrix}\dot{U}_* \\ \dot{\theta}_* R\end{bmatrix} dy\right\}[C_o]^{-1}\{q_o\} \tag{28}$$

Equation (28) can be rewritten as

$$T = p^2\{q_o\}^T[C_o]^{-T}[m_o][C_o]^{-1}\{q_o\} \tag{29}$$

where the corresponding degrees of freedom $\{q_o\}$ and the transformation matrix $[C_o]^{-1}$ have been given in Eqs. (25) and (27), respectively, and the mass matrix $[m_o]$ is

$$[m_o] = \rho_s A_s R^3 \times \begin{bmatrix} C_4M_1 & C_4M_2 & \sin\beta & M_3 & -C_3\sin\beta & C_4M_3 \\ & C_4M_4 & M_5 & M_6 & -C_3M_5 & C_4M_6 \\ & & \beta & -\beta^2/2 & 0 & -\beta^2/2 \\ & \text{symmetric} & & \beta^3/3 & 0 & \beta^3/3 \\ & & & & C_3\beta & C_3\beta^2/2 \\ & & & & & C_4\beta^3/3 \end{bmatrix} \tag{30}$$

where

$$M_1 = \beta/2 + \sin2\beta/4, \qquad M_5 = 1 - \cos\beta$$

$$M_2 = \sin2\beta/2, \qquad M_6 = \beta\cos\beta - \sin\beta$$

$$M_3 = 1 - \cos\beta - \beta\sin\beta, \qquad C_3 = \frac{Ip}{A_s R^2}$$

$$M_4 = \beta/2 - \sin2\beta/4, \qquad C_4 = 1 + C_3$$

Assembly Procedure and Theoretical Considerations

The finite element model of the curved packet of pretwisted blades having aerofoil cross sections is formulated as follows.

The shroud model is represented by a curved beam element, which is the same as what was used in Ref. 5. The blades are modeled by pretwisted beam elements with 12 DOF, which represent the coupled bending-bending-torsional vibrations.

The assembly procedure of the packet is the same as was used in Ref. 5; the difference being that the blade transformation matrix has 12 DOF since the blade elements are represented with 12 DOF beam elements.

The analysis is based on substructuring. That is to say, each component is considered individually and is then joined with the others by matching displacements and slopes in these coordinates where physical connections exist. Basic components and coordinates used are shown in Fig. 1.

Applications and Discussions

For a better and ideal representation of turbomachinery blade packets, the shroud is represented by curved beam elements, whereas the blades are represented by pretwisted aerofoil cross-section beam elements. To show the accuracy and improvement of this representation, several blade packets are tested experimentally.

In Table 2, experimental and theoretical results of a pretwisted blade packet are shown. There are some discrepancies between calculated and measured frequencies of about 3.5% and in one mode 6.9%. Some error was probably caused by uncertainty of Young's modulus, the density, and residual stresses in the test piece. The residual stresses were caused by pretwisting the blades in a small, manually operated torsion machine.

In Table 4, experimental and theoretical results of an aerofoil cross section 30-deg staggered and 30-deg pretwisted two-bladed packet under nonrotating conditions are shown. The comparisons of experimental and theoretical frequencies of the same packet under various rotational speeds are shown in Table 5.

Discrepancies can be seen between experimental and calculated values. The same reason that was explained earlier can be given for the causes of these discrepancies. It was concluded that present results are sufficiently accurate for engineering calculations, especially when the complex blade configurations are considered.

In Fig. 2, the increase of frequency parameter with disk rotational speed is shown. As mentioned in Ref. 6, there was a slight increase in the fundamental frequency ratio of a single blade with an increase in pretwist angles. This was due to the coupling between bending in the *yy* and *xx* directions since

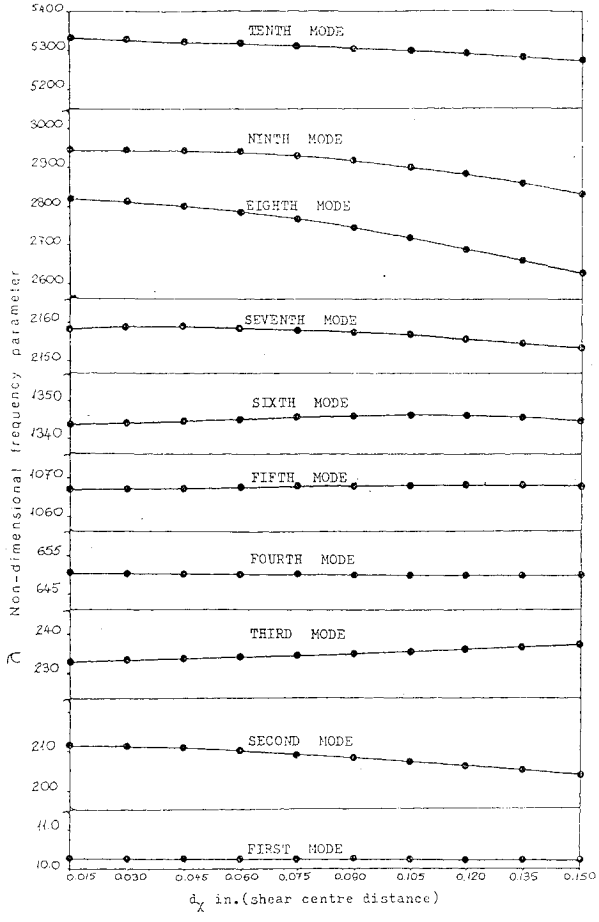

Fig. 6 Effect of shear center distance from the centroid on the nondimensional frequency parameters: α = 45 deg; L_r = 0.5; t = 1/32 in.; b = 1 in.

Table 4 Comparison of experimental and theoretical values of pretwisted two-aerofoil cross-section bladed packet[a]

Mode number	Frequency, Hz		
	Theoretical	Experimental	% error
1	95.5	97.0	−1.5
2	470.0	476.0	−1.2
3	490.4	501.0	−2.1
4	652.9	585.0	+11.4
5	822.4	829.0	−0.7
6	946.8	910.0	+4.0
7	1249.8	—	—
8	1622.2	1606.0	+1.0
9	1633.9	1671.0	−2.2
10	1912.8	—	—
11	2116.6	—	—
12	2490.5	2616.0	−4.7
13	3013.1	2927.0	+2.9
14	3354.9	3298.0	+1.7
15	3806.6	3867.0	−1.5

[a]Details of the blade packet are given in Table 3.

torsional movement was negligible. In the blade packet case, although all the motions are coupled through shroud interconnections, the fundamental mode is dominated by the blade vibration. Consequently, as in the single blade vibration case, when the rotational speed increases, the fundamental frequency also increases. It can be concluded that fundamental frequency increases with the increase of rotational speed and pretwist angle. The second mode corresponds to the batch mode, which is dominated by the shroud out-of-plane vibration. It can be seen that there is a decrease in the frequency parameter as the pretwist angle increases. This is due to the flexibility increase in the out-of-plane direction with the increase of pretwist, which causes a drop in the second frequency parameter. Third frequencies are torsional and out-of-plane coupled mode frequencies. This coupling increases with the increase in pretwist; consequently, the nondimensional frequency parameter also increases. As seen from Fig. 2, the third mode frequency of 90-deg pretwisted blade packets is higher than the third mode frequency of 45-deg pretwisted blade packets. For the fourth mode, the vibration is a coupled one between torsional and out-of-plane vibrations. The 45-deg pretwisted bladed packet mode is dominated by the torsional mode, whereas the 90-deg pretwisted bladed mode is dominated by the out-of-plane vibration. In the case of the fifth mode, the pretwist effect is still seen on the frequencies. The 90-deg pretwisted bladed packet mode is dominated by the out-of-plane coupled vibrations of the shroud and blade, whereas the 45-deg pretwisted blade packet mode is dominated by the in-plane coupled vibration of the shroud and blade.

A similar phenomenon, with different L_r ratio, can be seen in Fig. 3. When comparison is made between the two figures, it can be seen that in the stationary blade packet case an increase in L_r ratio or mass ratio decreases the fundamental frequency. In the rotational case, the percentage increase of the frequency increases with L_r ratio when the disk rotational speed increases. This is due to the increase of the centrifugal force effect of the shroud mass on the system. The conclusion can be drawn that all of the frequencies are increasing with the increase in rotational speed. The fundamental frequency increases when the pretwist, shroud length and rotational speed increases.

Figure 4 shows the effect of pretwist on the frequencies of the packet with different stagger angles. In the case of the first mode, the frequency parameter increases with the increase of pretwist angle but decreases with the stagger angle. The 90-deg staggered bladed packet is more flexible out of plane; consequently, the fundamental frequency decreases with an increase in stagger angle. However, an increase of pretwist makes the system stiffer; consequently, the funda-

Table 5 Comparison of experimental and theoretical values of a pretwisted packet with different rotational speeds

Mode number	500 rpm		1000 rpm		1500 rpm		2000 rpm	
	Theoretical	Experimental	Theoretical	Experimental	Theoretical	Experimental	Theoretical	Experimental
1	97.2	97	102.1	100	109.7	106	119.6	114
2	471.4		475.3		481.5		489.6	
3	491.7	506	495.6	507	502.0	509	510.5	512
4	653.6	586	655.4	587	658.2	589	661.5	591
5	823.8		827.5		832.3		836.9	
6	947.4	899	949.3	900	952.3	902	956.6	905
7	1250.2		1251.0		1252.2		1252.9	
8	1624.2	1603	1629.7	1608	1637.7	1615	1646.7	1628
9	1635.7		1641.0		1649.4		1660.5	
10	1913.0		1912.6		1909.6		1899.9	
11	2125.1		2147.8		2178.5		2209.5	
12	2490.9		2491.0		2487.2		2473.3	
13	3015.8	2902	3023.1	2912	3033.6	2925	3044.8	2938
14	3358.2	3270	3367.2	3272	3380.0	3276	3392.9	3292

mental frequency increases. For the second mode, there is a small increase in the frequency parameter with pretwist angles. For the 90-deg stagger angle, this mode is dominated by coupled out-of-plane shroud-blade vibrations, whereas for the 0-deg stagger angle, at the lower pretwist angle, this mode is dominated by coupled in-plane shroud-blade vibrations. On the contrary, at the higher pretwist angle, the mode becomes a coupled out-of-plane shroud and blade vibration. As seen from Fig. 4, this mode is more affected by the stagger angle than by pretwist. For the third mode, there is always a decrease with an increase of pretwist angle for the two cases. When the single blade vibration was analyzed in Ref. 6, it was noticed that the frequency of the second mode was decreasing with an increase of pretwist. It may be said that a similar phenomenon is happening here although there is coupling through shroud interaction. The fourth mode is also a coupled one and slightly dominated by the shroud vibration. These variations of frequency parameters are related to the flexibility of the system in the relevant direction, depending on the stagger angle and pretwist.

When the blades are pretwisted and have asymmetrical aerofoil cross sections, out-of-plane, in-plane, and torsional vibrations of the packet are coupled due to the blade configuration and noncoincidence of shear center and centroid of the cross section, as well as through the shroud interaction. As a result, they may not be easily synthesized by independent modes, and so it becomes more complex to predict these frequencies for a multibladed packed from a two-bladed packet inference diagram.

Figure 5 shows the inference diagram of a 15-deg pretwisted two-bladed packet. The independent frequencies of vibration of a pretwisted blade and shroud in-plane frequencies are shown in solid lines, whereas the packet frequencies are shown in broken lines. It can be seen that the packet frequency curves tend to asymptote to the blade frequencies, whereas shroud frequencies are, in turn, changing at every junction between the blade and shroud independent frequencies. This curve is useful in synthesizing the vibration characteristics and mode shapes of blade packets from the frequency characteristics of individual components.

Figure 6 illustrates the effect of the location of the shear center relative to the centroid. It can be seen that this effect becomes pronounced in the higher frequencies but does not markedly effect the lower frequencies.

Conclusions

The finite element model developed in this paper is found to be ideal for the vibration analysis of a pretwisted asymmetric cross-section blade packet under rotating and nonrotating conditions. It can be concluded that the fundamental frequency increases with an increase in rotational speed and pretwist. Higher modes are coupled through shroud interconnections between torsional and out-of-plane vibrations. In the stationary blade packet case, an increase in mass ratio decreases the fundamental frequency, whereas in the rotational case, it increases it. Staggered bladed packets are more flexible in the out-of-plane direction; consequently, the fundamental frequency decreases with an increase in stagger angle. For larger angles of pretwist, the inference diagrams may not be used in synthesizing the vibration characteristics from the frequency characteristics of individual components. The effect of the shear center distance from the centroid of a pretwisted blade packet becomes pronounced for the higher frequencies.

References

[1]Stodola, A., *Steam and Gas Turbines*, Vol. 12, McGraw-Hill, New York, 1927.

[2]Sezawa, K., "Vibration of Turbine Blades with Shrouding," *Philosophical Magazine*, 1933, pp. 164–174.

[3]Prohl, M. A., "A Method of Calculating Vibration Frequency and Stress of a Banded Group of Turbine Buckets," *Transactions of ASME*, Vol. 80, 1958, pp. 169–180.

[4]Thomas, J., and Belek, H. T., "Free Vibration of Blade Packets," *Journal of Mechanical Engineering Science*, Vol. 19, No. 1, 1977, pp. 13–21.

[5]Thomas, J., and Sabuncu, M., "Dynamic Analysis of Rotating Asymmetric Cross-Section Blade Packets," American Society of Mechanical Engineers, Paper 79-DET-93, Sept. 1979.

[6]Thomas, J., and Sabuncu, M., "Finite Element Analysis of Rotating Pretwisted Asymmetric Cross-Section Blades," American Society of Mechanical Engineers, Paper 79-DET-95, Sept. 1979.

[7]Ewins, D. J., "Bladed Disk Vibration—A Review of Techniques and Characteristics," International Conference on Recent Advances in Structural Dynamics, Southampton, England, UK, July 1980.

[8]Ewins, D. J., "Further Studies of Bladed Disk Vibration Effects Packeting," Inst. of Mech. Eng. Conference, "Vibration in Rotating Machinery," Cambridge, England, UK, 1980.

[9]Ewins, D.J., and Imregun, M., "Vibration Modes of Packeted Bladed Disk," *Journal of Vibration, Acoustics, Stress and Reliability in Design*, Vol. 106/179, April 1984.